# Narrowband-to-Broadband Conversion: Do Clouds Have Anomalous Absorption in the Visible Band?

*Z. Li and A. Trishchenko*
*Canada Center for Remote Sensing*
*Ottawa, Canada*

## Introduction

The Geostationary Operational Environmental Satellite (GOES) is a major source of space-borne observations for the Atmospheric Radiation Measurement (ARM) Program. The GOES-based radiation data processed by the National Aeronautics and Space Administration's Langley Research Center (NASA/LaRC) group (Minnis et al. 1995) are essential to many ARM studies, including investigations into the problem of cloud absorption anomaly (Smith et al. 1997; Cess et al. 1996; Imre et al. 1996; Cess et al. 1995). Since the GOES measurements are non-calibrated and cover narrow spectral bands, the quality of the inferred broadband fluxes needs assessment.

Narrowband-to-broadband conversion is required for estimating the broadband top of the atmosphere (TOA) radiation budget from narrowband measurements made by such operational radiometers as advanced very high-resolution radiometer (AVHRR), GOES, and meteorological satellite (METEOSAT). The simple assumption that visible albedo is equal to broadband albedo (Gruber and Winston 1978) is known to be inadequate due to the spectral dependence of atmospheric reflection and absorption and surface albedo, etc. Many conversion relationships have been established for GOES (Minnis and Harrison 1984), AVHRR (Wydick et al. 1987, Li and Leighton 1992, Hucek and Jacobowitz 1995) and METEOSAT (Vesperini and Fouquart 1994). Broadband albedo was usually expressed as a linear combination of visible and near infrared albedos. The coefficients of the regression were deduced from comparisons of narrowband and broadband measurements made from such platforms as Nimbus-7 (Wydick et al. 1987), NOAA (National Oceanic and Atmospheric Administration) 9 and 10 that carried both Earth Radiation Budget Experiment (ERBE) and AVHRR (Li and Leighton 1992), GOES (Minnis and Harrison 1984). Both scene-dependent and -independent regressional relationships of linear and non-linear formats were obtained.

For example, the relationship used by Minnis et al. (1995) for generating TOA radiation budget is

$$\alpha_{sw} = b_0 + b_1 \alpha_{VIS} + b_2 \alpha_{VIS}^2 + b_3 \ln(1/\mu_0) \qquad (1)$$

The objectives of this study are to

- validate the conversion relationship given by Eq. 1 using Scanner for Earth Radiation Budget (ScaRaB) data that include calibrated visible and broadband measurements (Kandel et al. 1994, Viollier et al. 1995)
- compare the relationships obtained from observations and model simulations. The comparison may be brought to bear on the recent claim that substantial cloud absorption anomaly may occur in the visible range.

## Conversion From Observations

To study the impact of the solar zenith angle (SZA) on the narrowband-to-broadband conversion, ScaRaB observations are analyzed for different SZA bins, separately. This was possible thanks to the orbit of the Russian Meteor-3/7 with the ScaRaB onboard. Over the entire possible range of 0° to 90° during a 7-month period, the SZA changes twice (for ascending and descending orbits). The relationship was studied at two ARM locales—Southern Great Plains (SGP) and Tropical Western Pacific (TWP)— using collocated and coincident narrowband and broadband albedos measured by ScaRaB from March through August 1994 (Figures 1 and 2). Note that their relationships are basically linear for all SZA bins. The slope of the regression between the two quantities depends on SZA. Except for large SZA, the slope generally increases with increasing SZA. Such a trend is well captured by a radiative transfer model as discussed below. Also worth noting is that the scattering of the data points tends to be large for low sun positions. This may be associated with 3-dimensional cloud effects and increased sensitivity to

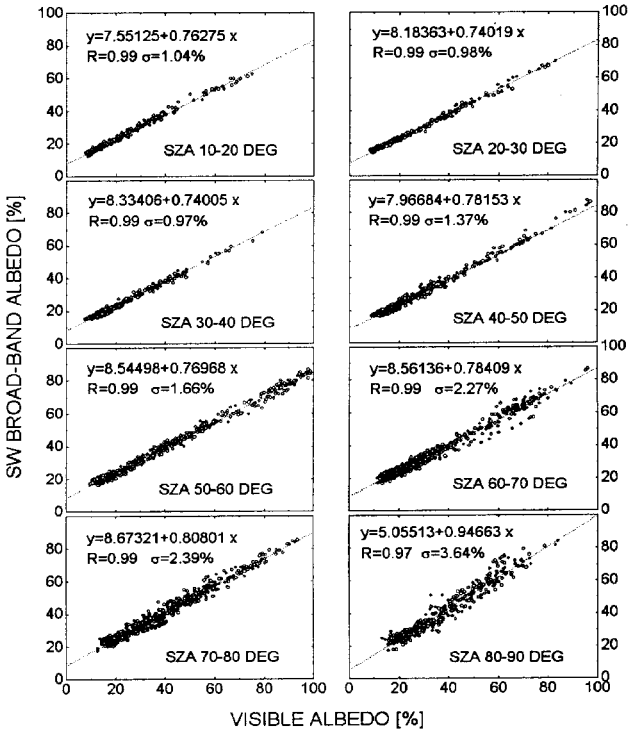


**Figure 1**. Visible narrowband to short-wave broadband ScaRaB albedo relationship over SGP/ARM locale (35.61-37.61°N, 96.5-98.5°W) from March to August 1994.

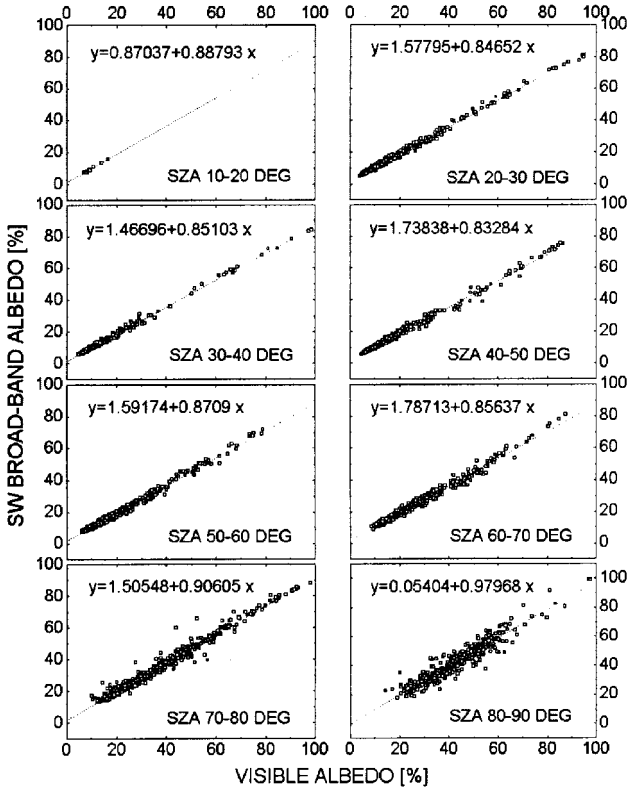


**Figure 2**. Visible narrowband to short-wave broadband ScaRaB albedo relationship over TWP site (1N-18, 164-166°E) from March to August 1994.

atmospheric absorbers. The relationship between the narrowband and broadband albedos and its dependence on the cosine of SZA ($\mu_0$) were parameterized as follows:

$$\alpha_{sw} = 7.64 - 2.551n\mu_0 - 1.47\ln^2\mu_0 + \alpha_{VIS}(0.753 - 0.008\ln\mu_0 + 0.0288\ln^2\mu_0) \quad (2)$$

for the SGP region and

$$\alpha_{sw} = 1.20 - 1.26\ln\mu_0 - 0.71\ln^2\mu_0 + \alpha_{VIS}(0.859 + 0.012\ln\mu_0 + 0.0261\ln^2\mu_0) \quad (3)$$

for the TWP region.

# Comparison of Observed and Modeled Narrowband-Broadband Relationship

The relationship derived from observations was further apprehended by means of radiative transfer modeling using a double-adding model (Masuda et al. 1995). The optical thicknesses for molecular scattering and absorbing atmospheric constituents were obtained from the LOWTRAN-7 program. We modeled the visible-short-wave albedo relationships for different land and ocean surfaces types and cloud conditions. The spectral and angular dependencies of land albedo for the SGP region followed the classification of land cover types used by the Clouds and Earth's Radiant Energy System (CERES) project based on Brieglib et al. (1986). The bulk of computations for the SGP was obtained over grassland and savanna types of surfaces. For the ocean, we used an albedo model given by Hansen et al. (1983) that was based on the parameterization of Cox and Munk wave-facets theory and Fresnel reflection. Cloud models include St,

Sc, Nb and Cu defined by Stephens (1979). We also used the continental and maritime aerosol models with different optical thickness varying from 0 to 1. For SGP simulations, the midlatitude summer and standard U.S. atmospheres were assumed except for temperature and humidity profiles, which were taken from measurements for April 1994 archived in CERES/ARM/GEWEX (CAGEX[a]) (Charlock and Alberta 1996). The average aerosol optical depth for April 1994 was close to 0.1 with a standard deviation of about 0.05. For the TWP site, we used a standard tropical model of the atmosphere with aerosol optical thickness around 0.1.

The results of modeling for SZAs of 80°, 60° and 76° for the TWP region are shown in Figure 3 and for the SGP region in Figure 4. The regression lines obtained from ScaRaB for the corresponding SZAs are also presented. The model results agree fairly well with ScaRaB observations. The model reproduces all the main features of the visible and broadband relationship in terms of intercept and slope magnitudes, increasing of the slope with SZA, and larger data scattering at low sun positions. We tested ScaRaB conversion algorithms using an independent dataset for September 1994. The results of testing are given in Table 1 which demonstrates clearly the advantage of using a SZA-dependent conversion model. The accuracy of broadband retrievals is improved, on average, by 10-12 W/m$^2$. The dependence on SZA might explain the strong latitude dependence of retrieval accuracy found by Hucek and Jacobowitz.

The conversion used for generating the GOES-based radiation product (Minnis et al. 1995) is shown in Figure 5, where GOES-7 visible albedos have been corrected to account for the small spectral difference between ScaRaB and GOES-7 visible channels and the differences in the angular correction schemes used for estimating irradiances from radiances (Trishchenko and Li 1997). The versions of GOES-7 ARM data issued on August 29/96 for April/94 data and in May/96 for July 1994 data were employed in Figure 5. The difference between the conversion algorithm established here and that used for GOES-7 can be as much as 10-15% at large SZAs. The GOES-7 conversion overestimates SW albedo for most of clear sky and partly cloudy scenes or cloudy scences with small or moderate albedos (<50-60%). As we show (Trishchenko and Li 1997), the inadequate visible narrowband-to-broadband conversion was partially responsible for the "enhanced cloud absorption" due to reduced TOA cloud radiative forcing.

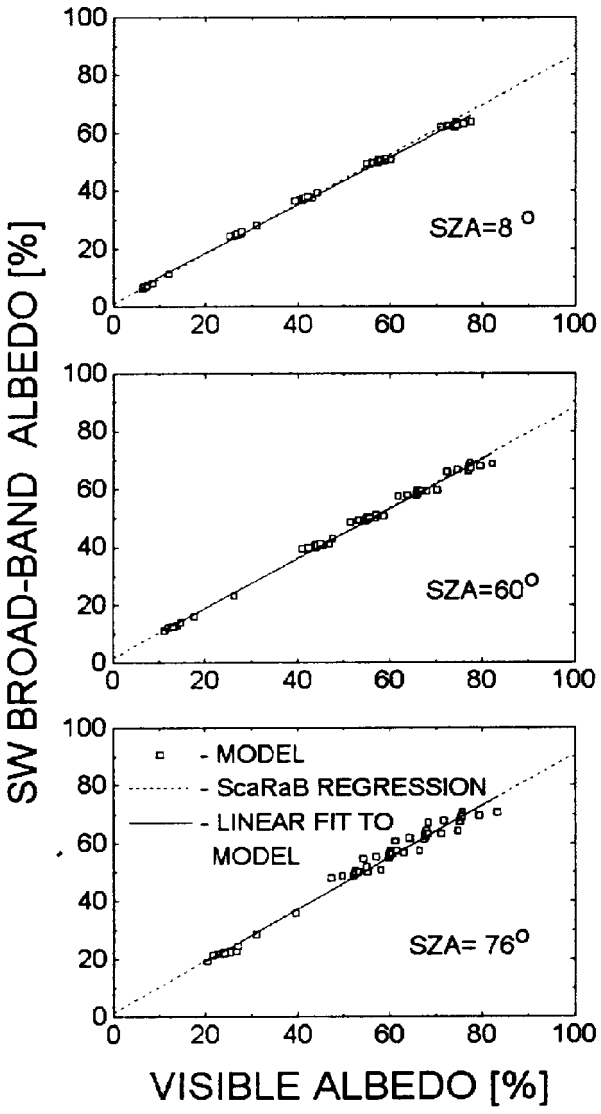


**Figure 3**. Comparison of modeling results and ScaRaB regression for the TWP oceanic region.

(a) CERES (Clouds and Earth's Radiant Energy System), ARM (Atmospheric Measurement Program), GEWEX (Global Energy and Water Experiment).

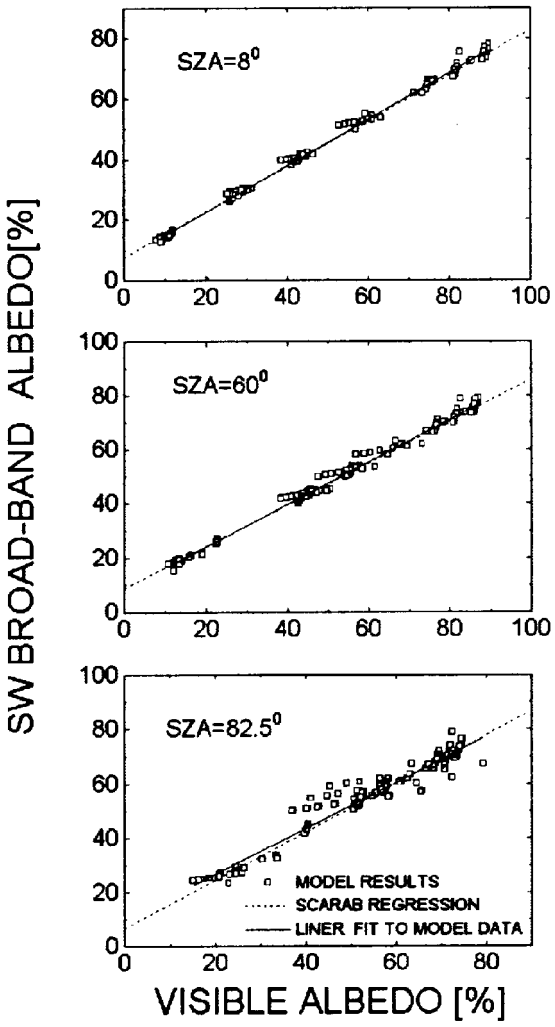


**Figure 4**. Comparison of modeling results and ScaRaB regression for the SGP/ARM locale.

**Table 1**. The statistics of independent comparison between retrieved and observed broadband. fluxes. ScaRaB METEOR-3/7. 1-30 September 1994.

| Region | ALBEDO (%) | | SW FLUX ($Wm^{-2}$) | |
|---|---|---|---|---|
| | mean | rms | mean | rms |
| SGP | -0.3<br>-1.2 | 1.2<br>1.6 | -3.4<br>-12.9 | 12.7<br>17.1 |
| TWP | -0.3<br>-1.3 | 1.4<br>1.9 | -4.5<br>-16.8 | 18.4<br>25 |

The SZA-dependent and -independent slopes and intercepts are given in the numerator and denominator, respectively.

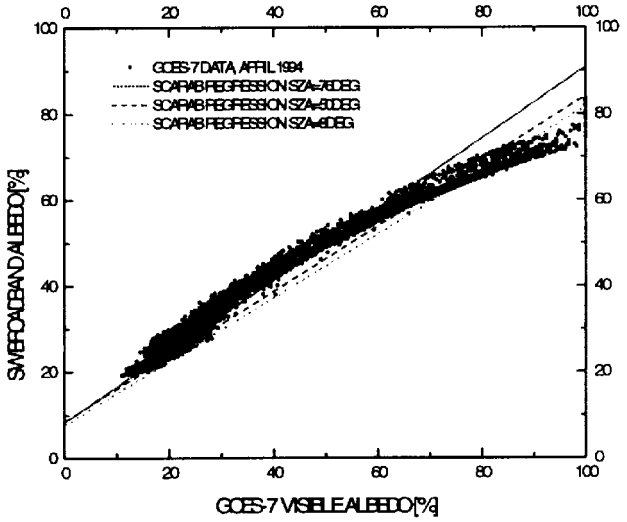


**Figure 5**. Comparison of GOES-7 and ScaRaB narrowband-to-broadband conversion.

# Summary

This study examines the conversion of satellite measurements from narrowband-to-broadband spectral intervals by means of radiative transfer modeling and use of synchronous data from ScaRaB/Meteor-3/7 for the SGP and TWP regions. It was shown that the algorithm derived from direct measurements of the ScaRaB radiometer for the ARM/ SGP locale agrees well with the results of radiative transfer computations, negating a possibility of an anomalous absorption in the visible band.

The narrowband-to-broadband relation is linear, with intercept and slope dependent on the solar zenith angle. Ignoring the solar zenith angle dependence introduces a retrieval error up to 10-12 $W/m^2$ on average in fluxes. Use of a conversion algorithm derived from ScaRaB data can lead to estimates of short-wave broadband albedo accurate to within 0.5% or 5 $W/m^2$ in terms of flux.

An inadequate conversion algorithm used in the retrieval of original GOES-based TOA data may cause an apparent "cloud absorption anomaly" due to reduced cloud radiative forcing at the TOA.

# References


Brieglib, B. P., P. Minnis, V. Ramanathan, and E. Harrison, 1986: Comparison of regional clear-sky albedos inferred from satellite observations and model computations. *J. Clim. Appl. Meteor*., **25**, 214-226.

Cess, R. D., M. H. Zhang, P. Minnis, L. Corsetti, E. G. Dutton, B. W. Forgan, D. P. Garber, W. L. Gates, J. J. Hack, E. F. Harrison, X. Jing, J. T. Kiehl, C. N. Long, J.-J. Moncrette, G. L. Potter, V. Ramanathan, B. Subasilar, C. H. Whitlock, D. F. Young, and Y. Zhou, 1995: Absorption of solar radiation by clouds: Observations versus models. *Science*, **267**, 496-499.

Cess, R. D., M. H. Zhang, Y. Zhou, X. Jing, and V. Dvortsov, 1996: Absorption of solar radiation by clouds: Interpretation of satellite, surface, and aircraft measurements. *J. Geophys. Res*., **D101**, No 18, 23299-23309.

Charlock, T. P., and T. L. Alberta, 1996: The CERES/ ARM/ GEWEX Experiment (CAGEX) for the retrieval of radiative fluxes with satellite data. *Bull. Amer. Meteor. Soc*. **77**, 2673-2683.

Gruber, A., and J. S. Winston, 1978: Earth-atmosphere radiative heating based on NOAA scanning radiometer measurements. *Bull. Amer. Meteor. Soc*., **59**, 1570-1573.

Hansen J. E., D. Russel, D. Rind, P. Stone, A. Lacis, L. Travis, S. Lebedeff, and R. Ruedy, 1983: Efficient three-dimensional global models for climate studies: Models I and II. *Mon. Wea. Rev*., **111**, 609-662.

Hucek, R., and H. Jacobowitz, 1995: Impact of scene dependence on AVHRR albedo models. *J. Atmos. Ocean. Technol*., **12**, 697-711.

Imre, D. G., E. H. Abramson, and P. H. Daum, 1996: Quantifying cloud-induced shortwave absorption: An examination of uncertainties and recent arguments for large excess absorption. *J. Appl. Meteorol*. **35**, 1991-2010.

Kandel, R. S., J-L. Monge, M. Viollier, L. A. Pakhomov, V. I. Adas'ko, R. G. Reitenbach, E. Raschke, and R. Stuhlmann, 1994: The ScaRaB project: Earth radiation budget observations from meteor satellites. *Adv. Space Res*., **14**, 47-57.

Li, Z., and H. G. Leighton, 1992: Narrowband to broadband conversion with spatially autocorrelated reflectance measurements. *J. Appl. Meteor*. **31**, 421-432.

Masuda, K., H. G. Leighton, and Z. Li, 1995: A new parameterization for the determination of solar flux absorbed at the surface from satellite measurements. *J. Clim.* **8**, 1615-1629.

Minnis, P., and E. F. Harrison, 1984: Diurnal variability of Regional Cloud and Clear-Sky Radiative Parameters Derived from GOES Data. Part III: November 1978 Radiative Parameters. *J. Clim and Appl. Meteor*., **23**, 1023-1051.

Minnis, P., W. L. Smith, D. P. Garber, J. K. Ayers, and D. R. Doelling, 1995: Cloud Properties Derived From GOES-7 for Spring 1994 ARM Intensive Observation Period Using Version 1.0.0 of Arm Satellite Data Analysis Program. *NASA Reference Publication* **1366**, 58.

Smith, W. L, L. Nguyen, and P. Minnis, 1997: Cloud Radiative Forcing Derived from ARM Surface and Satellite Measurements during ARESE and the spring ARM/UAV IOP. *9th Conference on Atmospheric Radiation*. Long Beach, California, pp. 1-4. American Meteorological Society, Boston, Massachusetts.

Stephens, G. L., 1978: Radiation profiles in extended water clouds. Part I Theory. *J. Atmos. Sci*., **35**, 2111-2122

Trishchenko, A., and Z. Li, 1997: Validation of GOES-7 TOA radiation budget for April and July 1994 ARM/IOP using ScaRab/Meteor-3/7 data. *Proceedings of the Seventh Atmospheric Radiation (ARM) Science Meeting*. CONF-970365, U.S. Department of Energy, Washington, D.C.

Vesperini, M., and Y. Fouquart, 1994: Determination of broad-band shortwave fluxes from the Meteosat visible channel by comparison to ERBE. *Beitr. Phys Atmosph*., **67**, N2, 121-131.

Viollier, M., R. S. Kandel, and P. Paberanto, 1995: Inversion and space-time-averaging algorithms for ScaRAB (Scanner for Earth Radiation Budget). Comparison with ERBE. *Ann. Geophys*. **13**, 959-968.

Wydick, J. E., P. A. Davis, and A. Gruber, 1987: Estimation of broadband planetary albedo from operational narrowband satellite measurements. *NOAA TR/NESDIS* **27**, 32.